An Interferometric view of Speckle Imaging

Olivier Leblanc[1], Matthias Hofer[2], Siddharth Sivankutty[3], Hervé Rigneault[2] and Laurent Jacques[1].

[1]ISPGroup, ICTEAM, UCLouvain, Belgium. [2]Institut Fresnel, Marseille, France. [3]Université de Lille, France

***Abstract*— Lensless endoscopy (LE) with multicore fibers (MCF) enables fluorescent imaging of biological samples at cellular scale. In this work, we show that the corresponding imaging process is tantamount to collecting multiple rank-one projections (ROP) of an Hermitian *interferometric* matrix—a matrix encoding a subsampling of the Fourier transform of the sample image. Specifically, each ROP of this matrix is achieved with the complex vector shaping the incident wavefront using a spatial light modulator (SLM), and, the image frequencies are taken at pairwise differences of the cores positions, allowing for as many frequencies as the square of the core number if there is no multiplicity. As for typical compressive sensing (CS) applications, we demonstrate that the sampling rate is directly connected to the sample structure when the SLM is configured randomly. For instance, a sparse sample in the spatial domain induces a low rank interferometry matrix. Interestingly, inspecting the separate dimensional conditions ensuring the specific restricted isometry properties of the two composing sensing models (the partial Fourier sampling of the interferometric matrix and the ROPs applied to it) in the observation of sparse images, we show in a simplified setting that a basis pursuit denoising (BPDN) program associated with an ℓ_1-fidelity cost provably provides a stable and robust image estimate.**

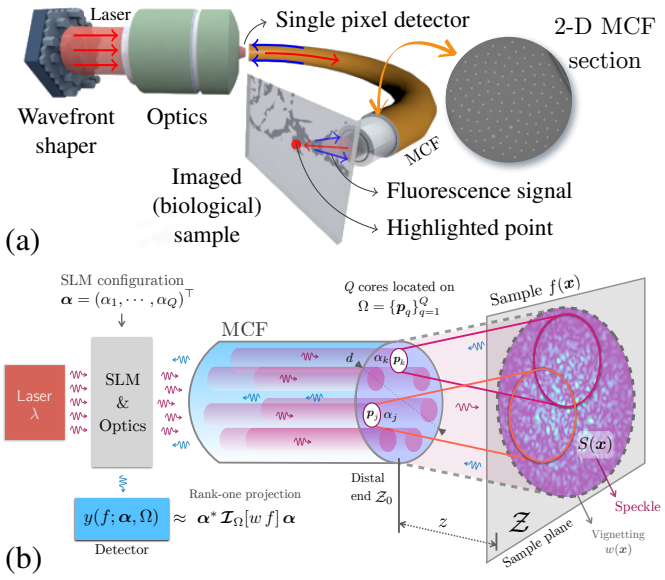

Figure 1: (a) Working principle of an MCF lensless endoscope with fiber cores aranged in Fermat's golden spiral and in raster scanning mode. (b) Interferometric LE and its link with ROPs of the interferometric matrix.

1 Introduction

Lensless endoscopy enables *in vivo* fluorescent imaging at a cellular scale [1, 2]. As illustrated in Fig. 1-(a), thanks to a proper calibration of the incoming light wavefront with a spatial light modulator (SLM) combined with scanning (galvanometric) mirrors (not represented), a lensless endoscope (LE) combined with a multicore fiber (MCF) usually images a 2D biological sample by raster scanning (RS) it with a focused beam illuminated from the MCF distal end; the light re-emitted by the fluorescent sample being collected and recorded for each focused spot location. Recently, a new scheme inspired by the compressive sensing theory [3] has been proposed. In this setting, which we refer to as speckle imaging (SI), the sample is illuminated with random speckles—achieved by randomly configuring the SLM—which mimics a compressive imaging system with random waveforms. While experimental evidence shows that SI allows for improved image reconstruction quality or reduced acquisition time compared to RS, it is not clear how to predict from which number of observations SI provides a stable and robust estimate of the observed sample. The randomness of the speckle illumination over the field-of-view (FOV) in the sample plane $\mathcal{Z}$—*i.e.*, the intensity of the interfering beams of the Q MCF cores—is indeed parametrized by only Q random variables. This complicates the analysis of such an illumination with the standard tools of CS theory (*e.g.*, the restricted isometry property – RIP) and limits the achievable imaging resolution. In this work we adopt a different approach; we show that, under a common far-field approximation, the sensing model of SI is factorized as a partial Fourier sensing of the sample image followed by rank-one projections of an *interferometric* matrix encoding this Fourier sampling. This allows us to characterize the sample complexity of the system, *i.e.*, the minimal number of SLM configurations (or speckle illuminations) required to estimate an accurate sample image.

2 Sensing model

Considering an MCF with diameter d and Q fiber cores (see Fig. 1-(b)) whose locations on the MCF distal end $\mathcal{Z}_0$ are in $\Omega := \{\boldsymbol{p}_q\}_{q=1}^Q \subset \mathbb{R}^2$, and assuming a planar sample in the plane $\mathcal{Z}$ at a distance z from $\mathcal{Z}_0$, by optically shaping the light wavefront with an SLM, we can set to $\alpha_q \in \mathbb{C}$ the complex amplitude of the electromagnetic field at each fiber core $\boldsymbol{p}_q$. Writing $\boldsymbol{\alpha} = (\alpha_1, \cdots, \alpha_Q)^\top \in \mathbb{C}^Q$ and $\boldsymbol{x} \in \mathbb{R}^2$ a point on $\mathcal{Z}$, under the far-field approximation $z \gg d^2/\lambda$ (with λ the laser wavelength) the illumination produced by the MCF on $\mathcal{Z}$ reads [4]

$$S(\boldsymbol{x};\boldsymbol{\alpha}) \approx \tfrac{1}{(\lambda z)^2}\, w(\boldsymbol{x}) \left|\textstyle\sum_{q=1}^Q \alpha_q e^{\frac{2\pi \mathrm{i}}{\lambda z} \boldsymbol{p}_q^\top \boldsymbol{x}}\right|^2,$$

where w is a smooth vignetting function—a Gaussian envelope with a diameter inversely proportional to the fiber cores diameter—determining the FOV. In RS mode, a focused beam can be obtained in $\mathcal{Z}$ when the Q fiber core locations in Ω are arranged in a Fermat's golden spiral shape [1]; we will restrict our analysis to this configuration. The LE collects a fraction $c \in (0, 1)$ of the light y globally re-emitted by the sample—as modeled by the fluorophore density map $f(\boldsymbol{x})$—under the

illumination S. For short time exposure and low intensity illumination, fluorescence theory provides (in a noiseless regime)

$$y(f;\boldsymbol{\alpha},\Omega) = c\int_{\mathbb{R}^2} S(\boldsymbol{x};\boldsymbol{\alpha})f(\boldsymbol{x})\mathrm{d}\boldsymbol{x}$$
$$= \sum_{j,k=1}^{Q} \alpha_j\alpha_k^* \int_{\mathbb{R}^2} e^{\frac{2\pi\mathrm{i}}{\lambda z}(\boldsymbol{p}_j-\boldsymbol{p}_k)^\top \boldsymbol{x}} w(\boldsymbol{x})f(\boldsymbol{x})\mathrm{d}\boldsymbol{x} \in \mathbb{R}_+,$$

with the number of collected photons y being Poisson distributed. Therefore, introducing the *interferometry* matrix $\boldsymbol{\mathcal{I}}_\Omega[g] \in \mathbb{C}^{Q\times Q}$ such that, for a function $g : \mathbb{R}^2 \to \mathbb{R}$, $(\boldsymbol{\mathcal{I}}_\Omega[g])_{jk} := \int_{\mathbb{R}^2} e^{\frac{2\pi\mathrm{i}}{\lambda z}(\boldsymbol{p}_k-\boldsymbol{p}_j)^\top \boldsymbol{x}} g(\boldsymbol{x})\mathrm{d}\boldsymbol{x}$ with $\boldsymbol{\mathcal{I}}_\Omega[g]$ Hermitian, assuming $c = 1$ and considering the scenario where we collect M LE observations $\boldsymbol{y} = (y_1,\cdots,y_M)^\top$, each associated with a specific $\boldsymbol{\alpha}_m$ for $1 \leqslant m \leqslant M$,

$$y(f;\boldsymbol{\alpha}_m,\Omega) = \boldsymbol{\alpha}_m^* \boldsymbol{\mathcal{I}}_\Omega[\bar{f}\,]\,\boldsymbol{\alpha}_m = \left\langle \boldsymbol{\alpha}_m\boldsymbol{\alpha}_m^*, \boldsymbol{\mathcal{I}}_\Omega\big[\bar{f}\,\big]\right\rangle_F,$$

with $\bar{f} := wf$ is the image f vignetted by w. Under a high photon counting regime, and gathering all possible noise sources in an additive term $\boldsymbol{n}$, we can thus compactly write the SI sensing as

$$\boldsymbol{y} = \boldsymbol{\mathcal{A}} \circ \boldsymbol{\mathcal{I}}_\Omega\big[\bar{f}\,\big] + \boldsymbol{n}, \text{ with} (\mathcal{A}[\boldsymbol{H}])_m := \boldsymbol{\alpha}_m^* \boldsymbol{H} \boldsymbol{\alpha}_m, \quad \text{for } \boldsymbol{H} = \boldsymbol{H}^* \text{ and } 1 \leqslant m \leqslant M. \tag{1}$$

We thus observe that (1) is tantamount to first sampling the Fourier transform of $\bar{f}$ over frequencies selected in the difference set $\mathcal{V} := \frac{2\pi}{\lambda z}(\Omega-\Omega) = \{\frac{2\pi}{\lambda z}(\boldsymbol{p}_k-\boldsymbol{p}_j)\}_{j,k=1}^{Q}$, and next performing M rank-one projections (ROP [5, 6]) of $\boldsymbol{\mathcal{I}}_\Omega[\bar{f}\,]$ as determined by $\mathcal{A}$ and the complex amplitude vectors $\{\boldsymbol{\alpha}_m\}_{m=1}^M$. Thus, the SI sensing corresponds to a specific interferometric system: assuming we collect enough ROP observations, we can potentially estimate the interferometry matrix $\boldsymbol{\mathcal{I}}_\Omega[\bar{f}\,]$. The system is thus equivalent to the radio-interferometry principles [7]—each fiber core playing somehow the role of a radio telescope and each entry of $(\boldsymbol{\mathcal{I}}_\Omega[\bar{f}\,])_{kl}$ probing the frequency content of $\bar{f}$ on the "*visibility*" $\nu_{jk} := \frac{2\pi}{\lambda z}(\boldsymbol{p}_k - \boldsymbol{p}_j)$.

3 Interferometric structural models

If one aims to image a vignetted sample that is K-sparse in the spatial domain, *i.e.*, it is composed of a few spikes as $\bar{f}(\boldsymbol{x}) = \sum_{i=1}^K \rho_i\delta(\boldsymbol{x}-\boldsymbol{x}_i)$ for $K \ll Q$, the entry "jk" of the interferometric matrix reads $\boldsymbol{\mathcal{I}}_\Omega\big[\bar{f}\big]_{jk} = \sum_{i=1}^K \rho_i e^{\mathrm{i}2\pi(\boldsymbol{p}_j-\boldsymbol{p}_k)^\top \boldsymbol{x}_i}$. We can therefore write the interferometric matrix as

$$\boldsymbol{\mathcal{I}}_\Omega\big[\bar{f}\big] = \sum_i \rho_i \boldsymbol{u}(\boldsymbol{x}_i)\boldsymbol{u}^*(\boldsymbol{x}_i), \quad \boldsymbol{u}(\boldsymbol{x})_j := e^{\mathrm{i}2\pi\boldsymbol{p}_j^\top \boldsymbol{x}},$$

which shows that it is low-rank with rank K. More generally, for a sample $\bar{f}$ that can be assumed sparsely represented in a collection of functions $\{\psi_k\}_{k=1}^d$ (*e.g.*, a wavelet basis for bandlimited function supported inside Ω), *i.e.*, $\bar{f}(\boldsymbol{x}) = \sum_{k=1}^d \rho_k\psi_k(\boldsymbol{x})$ with $\|\boldsymbol{\rho}\|_0 = K \ll d$, then

$$\boldsymbol{\mathcal{I}}_\Omega[\bar{f}] = \sum_{k|\rho_k\neq 0}^{K} \rho_k \boldsymbol{\mathcal{I}}_\Omega[\psi_k].$$

This last expression highlights that the interferometric matrix belongs to a subspace of dimension K. With this assumption, each noiseless observation becomes

$$y_m = \boldsymbol{\alpha}_m^* \boldsymbol{\mathcal{I}}_\Omega[\bar{f}]\boldsymbol{\alpha}_m = \sum_k \rho_k \boldsymbol{\alpha}_m^* \boldsymbol{\mathcal{I}}_\Omega[\psi_k]\boldsymbol{\alpha}_m.$$

Therefore, the sensing model can be recast as the linear CS model $\boldsymbol{y} = \boldsymbol{\Phi}\boldsymbol{\rho}$, with the subtle difference in the statistical distribution of the coefficients in $\boldsymbol{\Phi}$ that are not independent compared to classical CS.

4 Image reconstruction

Assuming the sample $\bar{f} \in \Omega$ is band-limited, we are interested in accurately estimating a sampling $\boldsymbol{f} \in \mathbb{R}^N$ of $\bar{f}$ We consider a discretisation of (1) that reads

$$\boldsymbol{y} = \boldsymbol{\mathcal{A}} \circ \tilde{\boldsymbol{\mathcal{I}}}_\Omega[\boldsymbol{f}] + \boldsymbol{n}, \text{with } \tilde{\boldsymbol{\mathcal{I}}}_\Omega[\boldsymbol{f}] = \boldsymbol{R}_{\tilde{\mathcal{V}}}\boldsymbol{F}\boldsymbol{f},$$

where $\boldsymbol{F}$ is the Fourier matrix and $\boldsymbol{R}_{\tilde{\mathcal{V}}} : \mathbb{C}^N \mapsto \mathbb{C}^{Q\times Q}$ is the restriction to the set $\tilde{\mathcal{V}}$ obtained as a Cartesian gridding of the (off-grid) difference set $\mathcal{V}$ (reached by nearest neighbors). From the factorization of this model, we first conclude that the set $\tilde{\mathcal{V}}$ should ideally be composed of as many distinct frequencies as possible (except for the zero frequency that has multiplicity Q) to improve our knowledge of $\boldsymbol{f}$. Interestingly, we can show numerically that Fermat's gold spiral arrangement ensures the unicity of the visibilities $\tilde{\nu}_{jk}$ when $j \neq k$, *i.e.*, $\tilde{\mathcal{V}}$ is composed of $Q(Q-1)+1$ distinct frequencies. In a noiseless scenario, we have shown that there exists a combination of $M_0 = O(Q^2)$ deterministic ROP observations that exactly recovers $\tilde{\boldsymbol{\mathcal{I}}}_\Omega[\bar{f}\,]$. Therefore, in a compressive setting, we could first leverage the low-complexity structure of $\tilde{\boldsymbol{\mathcal{I}}}_\Omega[\bar{f}\,]$—as induced from that of $\boldsymbol{f}$—to recover $\tilde{\boldsymbol{\mathcal{I}}}_\Omega[\boldsymbol{f}]$ from $M < M_0$ random complex ROPs, and then infer $\boldsymbol{f}$ from its $Q(Q-1)+1$ frequencies encoded in $\tilde{\boldsymbol{\mathcal{I}}}_\Omega[\boldsymbol{f}]$, this second step being similar to the inverse problem posed in radio-interferometry [7, 8]. In a simpler case where the cores are placed at all integer positions, the interferometric matrix is shown to be circulant and low-rank, *i.e.*, $\tilde{\boldsymbol{\mathcal{I}}}_\Omega[\boldsymbol{f}] = \mathcal{T} \circ \boldsymbol{F}\boldsymbol{f}$ where $\mathcal{T} : \mathbb{C}^N \mapsto \mathbb{C}^{N\times N}$ is the operator that turns a vector into a circulant matrix. In this situation, the sensing operator $\mathcal{B}$ respects a specific RIP-ℓ_2/ℓ_1 property over the set of sparse images—thus extending former approaches restricted to real sparse and low-rank matrices [5], and the RIP of random partial Fourier sensing characterized by $\tilde{\mathcal{V}}$ [9]. Proposition 4.1 shows that proving this RIP-ℓ_2/ℓ_1 for $\mathcal{B}$ implies we can reliably estimate it in a single basis pursuit denoising program (BPDN) with an ℓ_1 fidelity term. This happens with high probability if the vectors $\{\boldsymbol{\alpha}_m\}_{m=1}^M$ are random and sub-Gaussian, and both M and Q^2 are large compared to the sparsity level of $\boldsymbol{f}$.

Proposition 4.1 (ℓ_2/ℓ_1 instance optimality of BPDN ℓ_1)**.** *Let $\boldsymbol{\mathcal{B}} := \boldsymbol{\mathcal{A}} \circ \mathcal{T} \circ \boldsymbol{F}$ be an operator that respects the RIP$_{\ell_2/\ell_1}(k', \alpha_{k'}, \beta_{k'})$ for $k' \in \{K, k+K\}$ with $K > 2k$, and $\frac{1}{\sqrt{2}}\alpha_{k+K} - \beta_K\frac{\sqrt{k}}{\sqrt{K}} > \gamma > 0$, for some $\beta > 0$. Then, $\forall \boldsymbol{f} \in \mathbb{R}^N$, the estimate*

$$\hat{\boldsymbol{f}} \in \arg\min_{\boldsymbol{u}} \|\boldsymbol{u}\|_1 \ \text{ s.t.} \big\| \underbrace{\boldsymbol{\mathcal{B}}(\boldsymbol{f}) + \boldsymbol{n}}_{\boldsymbol{y}} - \boldsymbol{\mathcal{B}}(\boldsymbol{u})\big\|_1 \leqslant \epsilon$$

satisfies

$$\|\boldsymbol{f} - \hat{\boldsymbol{f}}\|_2 \leqslant C\frac{\|\boldsymbol{f} - \boldsymbol{f}_K\|_1}{\sqrt{K}} + D\frac{\epsilon}{m}$$

The current theoretical derivations are accompanied by numerical and experimental reconstruction results (not shown in this abstract) that suggest Proposition 4.1 may also hold when relaxing the cited assumptions. Additionnally, this may extend to other optimisation problems like LASSO [10] or lagrangian formulations with various regularization terms (ℓ_1 in the identity or orthonormal basis, total variation).

References

[1] Siddharth Sivankutty, Viktor Tsvirkun, Olivier Vanvincq, Géraud Bouwmans, Esben Ravn Andresen, and Hervé Rigneault. Nonlinear imaging through a Fermat's golden spiral multicore fiber. *Optics Letters*, 43(15):3638, 2018.

[2] Esben Ravn Andresen, Siddharth Sivankutty, Viktor Tsvirkun, Géraud Bouwmans, and Hervé Rigneault. Ultrathin endoscopes based on multicore fibers and adaptive optics: status and perspectives. *Journal of Biomedical Optics*, 21(12):121506, 2016.

[3] Emmanuel J Candès, Justin K Romberg, and Terence Tao. Stable signal recovery from incomplete and inaccurate measurements. *Communications on Pure and Applied Mathematics*, LIX:1207–1223, 2006.

[4] Stéphanie Guérit, Siddharth Sivankutty, John Aldo Lee, Hervé Rigneault, and Laurent Jacques. Compressive lensless endoscopy with partial speckle scanning. 2021. (submitted).

[5] Yuxin Chen, Yuejie Chi, and Andrea J Goldsmith. Exact and stable covariance estimation from quadratic sampling via convex programming. *IEEE Transactions on Information Theory*, 61(7):4034–4059, 2015.

[6] T Tony Cai, Anru Zhang, et al. Rop: Matrix recovery via rank-one projections. *Annals of Statistics*, 43(1):102–138, 2015.

[7] Yves Wiaux, Laurent Jacques, Gilles Puy, Anna MM Scaife, and Pierre Vandergheynst. Compressed sensing imaging techniques for radio interferometry. *Monthly Notices of the Royal Astronomical Society*, 395(3):1733–1742, 2009.

[8] R. E. Carrillo, J. D. McEwen, and Y. Wiaux. Sparsity Averaging Reweighted Analysis (SARA): A novel algorithm for radio-interferometric imaging. *Monthly Notices of the Royal Astronomical Society*, 426(2):1223–1234, 2012.

[9] Simon Foucart and Holger Rauhut. A mathematical introduction to compressive sensing. *Bull. Am. Math*, 54(2017):151–165, 2017.

[10] Ewout van den Berg and Michael P. Friedlander. Probing the pareto frontier for basis pursuit solutions. *SIAM Journal on Scientific Computing*, 31(2):890–912, 2009.